(Received 6 April 2024, Accepted 27 May 2024, Scheduled 7 June 2024)

Broadband Cross-Coupled Filter Based on CPW Structure and Triangular SIW Resonant Cavity

Xiaohei Yan and Minjie Guo*

School of Mathematics, Physics, and Electronic Information Engineering
Guangxi Minzu Normal University, Chongzuo 532200, China

ABSTRACT: This paper proposes a cross-coupled filter that utilizes a coplanar waveguide (CPW) resonator and triangular substrate-integrated waveguide (TSIW) resonant cavities. The filter consists of a CPW resonator etched on the upper metal surface of a second-order triangular SIW resonant cavity. By adjusting the dimensions of the CPW resonator and optimizing the width of the inductive coupling window, precise control can be achieved over cross-coupling between resonators, enabling fine-tuning of both filter bandwidth and transmission zero placement. Simulation and test results indicate that the filter has a center frequency of 11.85 GHz, a −3 dB bandwidth of 1.82 GHz, a relative bandwidth of 15.4%, an insertion loss of −0.9 dB in the passband, a return loss over 15 dB, and a transmission zero point located at 15 GHz. The filter has a simple structure, wide bandwidth, low insertion loss, small circuit size, and a flexible and controllable transmission zero point, making it potentially valuable for various applications.

1. INTRODUCTION

Filters are essential in wireless transceiver systems to eliminate noise and maintain RF system stability, thereby significantly impacting wireless communication system transmission quality. Substrate integrated waveguides (SIWs) have become a popular choice for filter design due to their high-quality factor, low cost, low loss, and easy planar integration [1–6]. With the rapid development of modern microwave communication systems, cross-coupling technology is widely used in microwave filters to meet the requirements of miniaturization, low cost, high selectivity, strong out-of-band rejection, flexible and controllable transmission zero position, and other performance specifications. SIW cross-coupled filter has gained the attention of many researchers [7–13] due to its ability to meet the aforementioned requirements while retaining the advantages of SIW.

Re. [7] demonstrated the negative coupling between two SIW resonator cavities in a single layer by etching an S-slot between them. This structure was utilized to create a 4th-order cross-coupled filter using four SIW resonators, resulting in quasi-elliptical characteristics. However, the proposed structure does not aid in filter miniaturization. In [8], the negative coupling between two resonant cavities was achieved by etching grounded coplanar lines on the upper metal surface of a circular substrate integrated waveguide (SIW) resonant cavity. This structure was utilized to create a third-order cross-coupled filter using three circular SIW resonators, resulting in one transmission zero. However, the shape of the filter is unique, and its proposed structure did not aid in the miniaturization of the filter. Ref. [9] describes a method for achieving the hybrid electromagnetic coupling between adjacent SIW cavities by combining three slot lines on the top metal plane of the SIW with inductive windows between adjacent SIW cavities. This structure was used to realize a third-order cross-coupled filter with two transmission zeros and improved selectivity. It is important to note that the order of the filter must be consistent with the number of resonant cavities used. Ref. [10] implemented mixed-coupling (MC) in the design of substrate-integrated waveguide (SIW) cross-coupled filters with novel inter-digital slot lines (ISL). The filter exhibits two transmission zeros and quasi-elliptical characteristics. However, the number of resonant cavities cannot be reduced. Ref. [11] proposes a post-loaded electric coupling-enhanced structure that improves the electric coupling between two SIW resonators. A 4th-order cross-coupled filter is designed using this structure, which has two transmission zeros and quasi-elliptic characteristics. However, the filter has a high insertion loss. Ref. [12] reports a novel realization of a frequency-dependent coupling (FDC) structure that can achieve both positive and negative slopes. The FDC consists of two coupled, stepped-impedance grounded coplanar waveguides with open ends. This structure is used to design a third-order triplet cross-coupled filter. The filter has two transmission zeros in the upper rejection band, but its insertion loss is also high. In [13], a quasi-elliptic filter with controllable electric and magnetic mixed-coupling based on substrate-integrated waveguide cavity resonators using a two-layer printed circuit board process is presented. The design scheme combines an embedded short-ended strip line with a conventional inductive window between two cavities to create mixed-coupling. This allows for separate control of electric and magnetic coupling by adjusting the width of the strip line and the inductive window. Additionally, a controllable transmission zero can be produced below or above the passband. However, this filter has a double-

* Corresponding author: Minjie Guo (guominjie@gxnun.edu.cn).

layer structure, which increases the filter's size and manufacturing difficulty.

Most of the filters proposed in the above literature use conventional rectangular SIW resonant cavities for filter design, which have a fixed structural form and are not suitable for some occasions with special circuit shapes. The proposed coupling structures mainly achieve hybrid or electrical coupling, which cannot reduce the number of resonant cavities used and cannot realize filter miniaturization. This study proposes a cross-coupled filter based on a CPW structure and a triangular SIW resonant cavity. The filter enriches the structural form of cross-coupled filters and realizes a third-order filter with controllable transmission zero using only two resonance cavities. This reduces the number of resonance cavities used and achieves miniaturization of the filter to some extent. The filter developed in this study has a simple structure, wide bandwidth, low insertion loss, small circuit size, and flexible and controllable transmission zero, making it suitable for various applications.

2. STRUCTURE OF THE FILTER

The filter utilizes a substrate-integrated waveguide structure with a single layer. Fig. 1 displays the three-dimensional structure of the filter, which consists of two metal layers and a dielectric layer. The dielectric layer is made of ZYF300CA-P, which has a relative permittivity of 3, a loss tangent of 0.0018, and a thickness of 0.762 mm. The filter has two isosceles right-angled triangular SIW (TSIW) resonance cavities, both of which operate in the TM_{120}/TM_{210} mode. In the co-layer planar coupling design of SIW filters, the resonant cavities are connected through an inductive coupling window. Additionally, a CPW structure is etched between the two SIW resonant cavities to form a new resonator that cross-couples with the two cavities. The filter utilizes a coplanar waveguide transition structure at both input and output ports to ensure impedance matching with the source and load. The upper metal surface dimensions of the filter are shown in Fig. 2. After optimizing the simulation using HFSS software, the final structural parameters of the filter are presented in Table 1.

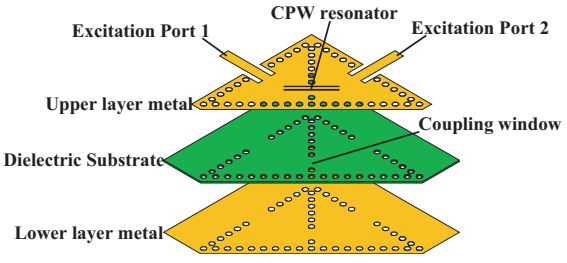

FIGURE 1. Structure of the filter.

TABLE 1. Structural parameters of the filter (unit: mm).

$a = 16.55$	$W_1 = 1.88$	$P = 1.84$	$d = 1$
$m = 2$	$g = 0.9$	$W_2 = 4$	$c = 3.7$
$L = 8.39$	$W_3 = 0.68$	$s = 0.2$	

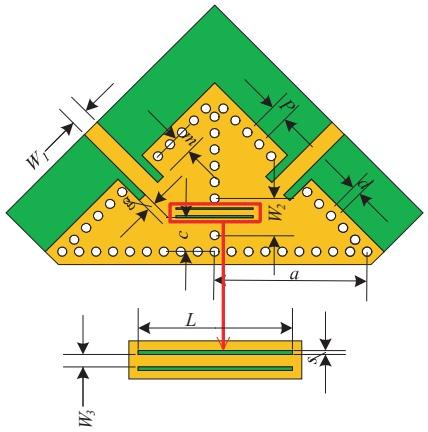

FIGURE 2. Dimensional drawing of the upper metal surface of the filter.

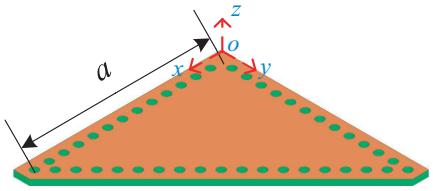

FIGURE 3. Schematic structure of isosceles right-angle TSIW resonant cavity.

3. FILTER DESIGN AND PRINCIPLE ANALYSIS

3.1. Isosceles Right-Angle Triangle SIW Resonant Cavity Theory

Figure 3 displays a schematic diagram of an isosceles right-angled TSIW resonant cavity. The dimensions of the cavity are determined by the right-angled edge dimension a. Resonant cavities can generally excite TE_{mnl} and TM_{mnl} modes, and their field components in each direction can be expressed as follows:

$$\begin{cases} \text{TM}: & H_x = \frac{j\omega\varepsilon}{k^2-k_z^2}\frac{\partial E_z}{\partial y}, \quad H_y = -\frac{j\omega\varepsilon}{k^2-k_z^2}\frac{\partial E_z}{\partial x}, \quad H_z = 0 \\ & E_x = -\frac{jk_z}{k^2-k_z^2}\frac{\partial E_z}{\partial x}, \quad E_y = -\frac{jk_z}{k^2-k_z^2}\frac{\partial E_z}{\partial y}, \\ & E_z = A_{mnl}T\cos(k_z z) \\ \text{TE}: & E_x = -\frac{j\omega\mu}{k^2-k_z^2}\frac{\partial H_z}{\partial y}, \quad E_y = \frac{j\omega\mu}{k^2-k_z^2}\frac{\partial H_z}{\partial x}, \quad E_z = 0 \\ & H_x = -\frac{jk_z}{k^2-k_z^2}\frac{\partial H_z}{\partial x}, \quad H_y = -\frac{jk_z}{k^2-k_z^2}\frac{\partial H_z}{\partial y}, \\ & H_z = B_{mnl}T\sin(k_z z) \end{cases} \tag{1}$$

where A_{mnl} and B_{mnl} represent arbitrary amplitude constants; T is the wave function to be solved; k is the wave number in the resonant cavity; and k_z is the component of the wave number in the z-direction. The variables μ and ε represent the magnetic permeability and dielectric constant of the propagation medium, respectively, and are defined as $\mu = \mu_0\mu_r$ and $\varepsilon = \varepsilon_0\varepsilon_r$. In this paper, the thickness of the resonant cavity studied is much smaller than its side length. Since the resonant cavity's length in the z-direction is very small, we can assume that there is no change in the field pattern along that direction. Therefore, the wave number component in the z-direction, k_z,

can be considered zero. By substituting $k_z = 0$ into the formula for the TE mode in Eq. (1), we can calculate the magnetic field in the z-direction of the TE mode, which is H_z =0. Since all other field components are also calculated from H_z, there are no TE modes in the resonant cavity under study. Therefore, only TM_{mn0} modes exist in the resonant cavity at this point. Similarly, by substituting $k_z = 0$ into the formula for the TM mode in Eq. (1), the field components of the TM_{mn0} mode in each direction can be obtained as:

$$\begin{cases} E_z = A_{m,n,0} T(x,y) \\ H_x = \frac{j}{\omega\mu}\frac{\partial E_z}{\partial y} \\ H_y = \frac{-j}{\omega\mu}\frac{\partial E_z}{\partial x} \\ H_z = E_x = E_y = 0 \end{cases} \tag{2}$$

In the theoretical derivation, the upper and lower metals of the TSIW resonant cavity can be regarded as ideal electric walls, and the metalized through-hole can also be approximated as an electric wall, so the boundary conditions to be satisfied for this resonant cavity are:

$$E_z|_{x=0} = 0, \quad E_z|_{y=0} = 0, \quad E_z|_{x=a-y} = 0 \tag{3}$$

By solving the Helmholtz equation $\nabla^2 T + k^2 T = 0$ satisfying the boundary condition (3), the wave function of the TM_{mn0} mode can be obtained as follows:

$$T_{m,n,0}(xy) = \sin\frac{m\pi x}{a_{eff}} \sin\frac{n\pi y}{a_{eff}} - \sin\frac{n\pi x}{a_{eff}} \sin\frac{m\pi y}{a_{eff}} \tag{4}$$

where a_{eff} is the equivalent length of the right-angled side of the isosceles right-angle TSIW resonant cavity, and m and n need to satisfy the conditions of $m \neq 0$, $n \neq 0$, and $m \neq n$. It should be noted that the m and n here are different from the frequency calculation formula of the rectangular cavity, and the exchange of the m and n numbers will not produce a new mode, i.e., the TM_{mn0} and TM_{nm0} denote the same mode in the isosceles right-angle TSIW resonant cavity. The transverse field component of the isosceles right-angle TSIW resonant cavity can be obtained by solving Eq. (2) as:

$$\begin{aligned} E_z &= A_{m,n,0}\left(\sin\tfrac{m\pi x}{a_{eff}} \sin\tfrac{n\pi y}{a_{eff}} - \sin\tfrac{n\pi x}{a_{eff}} \sin\tfrac{m\pi y}{a_{eff}}\right) \\ H_x &= \tfrac{j\pi A_{m,n,0}}{\omega\mu a_{eff}}\left(n\sin\tfrac{m\pi x}{a_{eff}} \cos\tfrac{n\pi y}{a_{eff}} - m\sin\tfrac{n\pi x}{a_{eff}} \cos\tfrac{m\pi y}{a_{eff}}\right) \\ H_y &= \tfrac{-j\pi A_{m,n,0}}{\omega\mu a}\left(m\sin\tfrac{n\pi y}{a_{eff}} \cos\tfrac{m\pi x}{a_{eff}} - n\sin\tfrac{m\pi y}{a_{eff}} \cos\tfrac{n\pi x}{a_{eff}}\right) \end{aligned} \tag{5}$$

After obtaining the wave function expression, the resonant wavelength of the resonant cavity can also be found as:

$$\lambda_{mn0} = \frac{2a_{eff}}{\sqrt{m^2+n^2}} \tag{6}$$

Ultimately, the resonant frequency of the isosceles right-angle TSIW resonant cavity with electric walls on all three sides of the desired solution is:

$$f_{mn0} = \frac{\sqrt{m^2+n^2}}{2a_{eff}\sqrt{\varepsilon\mu}} \tag{7}$$

where $m = 1, 2, 3, \ldots$, $n = 1, 2, 3, \ldots$, and $m \neq n$.

It can be seen that the main mode of the isosceles right-angled TSIW resonant cavity is TM_{120}/TM_{210} mode, which resonates at the frequency:

$$f_{120} = f_{120} = \frac{\sqrt{5}}{2a_{eff}\sqrt{\varepsilon\mu}} \tag{8}$$

The equivalent edge length a_{eff} in Eq. (8) can be obtained by the following equation [2]:

$$a_{eff} = a - \frac{d^2}{0.95P} \tag{9}$$

where d represents the diameter of the metal via hole, and P represents the distance between two metal via holes. The filter designed in this study is based on the main mode of an isosceles right-angle TSIW resonant cavity. The center frequency of the filter is initially taken as 11.8 GHz and set to $d = 1$ mm and $P = 1.84$ mm, and $a \approx 17$ mm is calculated using Eqs. (8) and (9).

3.2. Cross-Coupling Theory

Figure 4 shows the coupling topology of the filter, which consists of three resonators. Resonators 1 and 3 are SIW resonators, while resonator 2 is the CPW resonator etched on the metal upper surface of the SIW resonant cavity.

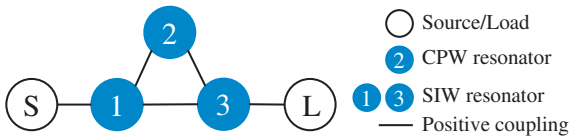

FIGURE 4. Coupling topology of the filter.

The coupling matrix of the filter can be expressed as:

$$\begin{bmatrix} 0 & M_{S1} & 0 & 0 & 0 \\ M_{S1} & M_{11} & M_{12} & M_{13} & 0 \\ 0 & M_{12} & M_{22} & M_{23} & 0 \\ 0 & M_{13} & M_{23} & M_{33} & M_{3L} \\ 0 & 0 & 0 & M_{3L} & 0 \end{bmatrix} \tag{10}$$

The filter's coupling matrix was extracted using the CoupleFil software, based on its final S-parameter profile. The matrix is presented below:

$$\begin{bmatrix} 0 & 0.973 & 0 & 0 & 0 \\ 0.973 & 0.044 & 0.892 & 0.189 & 0 \\ 0 & 0.892 & -0.202 & 0.892 & 0 \\ 0 & 0.189 & 0.892 & 0.044 & 0.973 \\ 0 & 0 & 0 & 0.973 & 0 \end{bmatrix} \tag{11}$$

According to the theory of related literature [6], the position of the transmission zero point can be determined by the following equation:

$$\Omega = \frac{M_{12}M_{23}}{M_{13}-M_{22}} = \frac{1}{FBW}\left(\frac{\omega}{\omega_0} - \frac{\omega_0}{\omega}\right) \tag{12}$$

where Ω represents the normalized angular frequency, and FBW represents the relative bandwidth.

If Ω is less than zero and ω less than ω_0, the CPW resonator will be coupled to the two SIW resonators in the opposite state. One resonator will be positively coupled and the other negatively coupled, resulting in $M_{12}M_{23}$ being less than zero. As a result, a transmission zero will be located on the left side of the filter's passband.

If Ω is greater than zero and ω greater than ω_0, the CPW resonator is coupled to the same state as the two SIW resonators, resulting in positive coupling ($M_{12}M_{23} > 0$). This leads to a transmission zero located on the right side of the filter's passband.

In our design, the CPW resonator is positively coupled to both SIW resonators. Therefore, a transmission zero will be located to the right of the filter's passband.

According to the theory presented above, the filter structure proposed in this study can more effectively achieve a third-order filter with a single transmission zero.

4. RESULTS AND ANALYSIS

4.1. Effect of W_3 Variation on Filter Performance

Figure 5 shows the filter S-parameter curves for different W_3 sizes. It is evident that the transmission zeros on the right side of the filter passband shift towards higher frequencies as the W_3 size increases. The increase in W_3 size causes a decrease in magnetic coupling (M_{13}) between the two TSIWs and an increase in coupling (M_{12} and M_{23}) between the CPW resonator and the two TSIW resonators. Therefore, the position of the transmission zeros of the filter can be adjusted by resizing W_3.

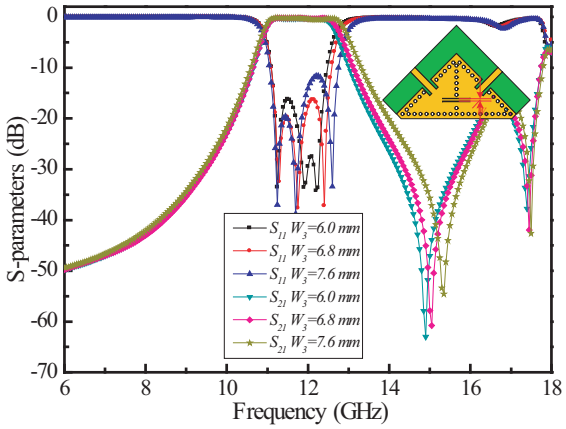

FIGURE 5. S-parameter curves of the filter for different W_3 dimensions.

4.2. Effect of L Variation on Filter Performance

Figure 6 shows the S-parameter curves of the filter for different L dimensions. It is evident that the passband and transmission zeros of the filter shift towards the low-frequency direction as the L size increases. This is due to the decrease in the resonant frequency of the CPW resonator caused by the increase in L size. Therefore, adjusting the L size can modify the passband and transmission zero positions of the filter.

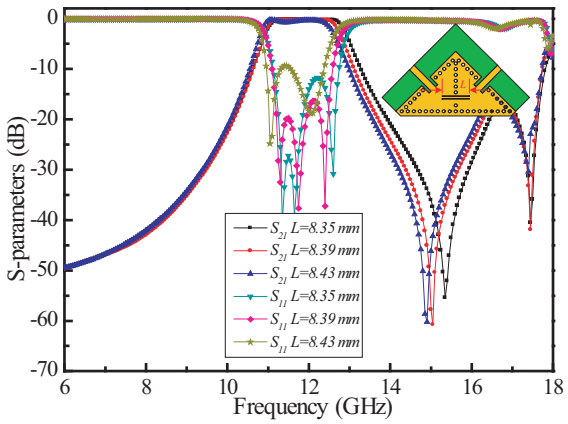

FIGURE 6. S-parameter curves of the filter for different L dimensions.

4.3. Effect of W_2 Variation on Filter Performance

Figure 7 shows the S-parameter curves of the filter with varying W_2 dimensions. The position of the transmission zero on the right side of the filter passband and the passband itself both shift towards the high-frequency direction as the W_2 size decreases. This is due to the decrease in magnetic coupling M_{13} between the two TSIWs caused by the reduction in W_2 size. Thus, adjusting the size of W_2 allows for the adjustment of both the passband position and the position of the transmission zero point of the filter.

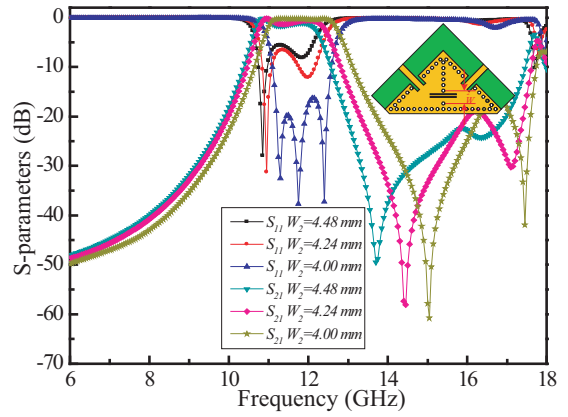

FIGURE 7. S-parameter curves of the filter for different W_2 dimensions.

4.4. Group Time Delay Characterization and Phase Characterization of the Filter

Figure 8 displays the phase characteristic curves of the S_{21} parameter of the filter. It is evident that the linearity of the phase characteristic of the filter is superior in the passband. Fig. 9 displays the group delay curves of the filter. It is evident that the group delay of the filter is less than 0.75 ns in the passband, and the maximum group delay variation is only 0.24 ns. At the same time, the filter exhibits a negative time delay at the trans-

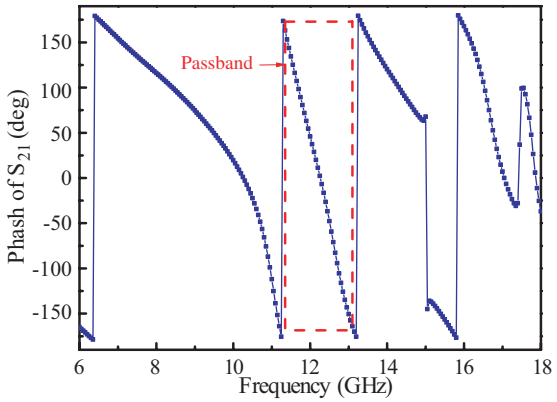

FIGURE 8. The phase characteristic curves of the S_{21} parameter.

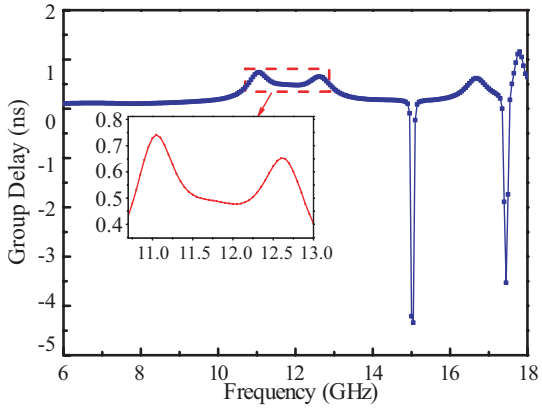

FIGURE 9. The group delay curve of the filter.

TABLE 2. Comparison with similar filters in the literature.

Refs.	Single layer	f_0 (GHz)	FBW (%)	Order	Insertion Loss (dB)	Size (λg^2)	TZ below, above f_0
[7]	√	20.5	3.4	4	0.9	2.16	1, 1
[8]	√	14.3	1.5	3	2.9	1.56	1, 0
[9]	√	10	8.9	3	1.6	1.87	1, 1
[10]	√	5.25	5.8	3	1.2	1.95	1, 1
[11]	√	5.8	2.5	4	6.4	2.28	1, 1
[12]	√	10	4.1	3	1.7	1.61	0, 2
[13]	×	27	7.4	4	2.1	2.41	1, 2
This work	√	11.85	15.4	3	0.9	1.3	0, 1

mission zero point, which is consistent with the characteristics of an asymmetric frequency response filter.

4.5. Test Results of the Filter

Based on the dimensions listed in Table 1, the physical filter underwent processing using the PCB method. To conduct the physical test, SMA-KHD coaxial connectors must be soldered onto the input and output ports of the filter and then connected to an Agilent E8363C model network vector analyzer for measurement. The simulated and measured results of the S-parameters of the filter are presented in Fig. 10. The measured and simulated S-parameter curves show a consistent overall trend. The filter has a center frequency of 11.85 GHz, a -3 dB bandwidth of 1.82 GHz, a relative bandwidth of 15.4%, a return loss over 15 dB, and a transmission zero located at 15 GHz. The simulation shows an insertion loss in the passband about -0.3 dB, while the measurement shows a 0.6 dB lower insertion loss than the simulation. The disparity between the measured and simulated values is primarily due to processing errors, dielectric loss, and conversion structure loss.

4.6. Comparison with Similar Filters in the Literature

Table 2 compares the performance of the filter proposed in this paper with the SIW filters in references. The proposed filter exhibits advantages in insertion loss, relative bandwidth, size,

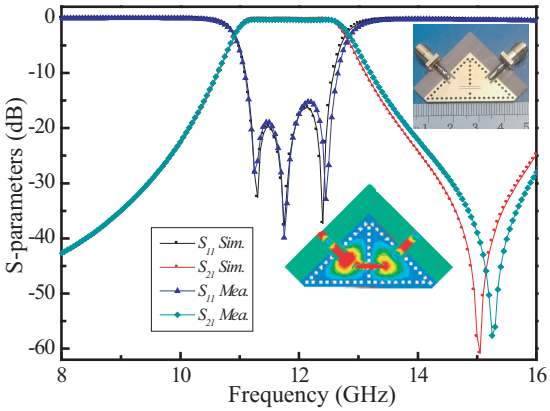

FIGURE 10. Simulation results and test results of the S-parameters of the filter.

and controllability of transmission zeros. Additionally, the used design methodology is simple and easy to implement.

5. CONCLUSIONS

This study proposes a cross-coupled filter based on a CPW structure and a triangular SIW resonant cavity. The filter enriches the structural form of cross-coupled filters and realizes a third-order filter with controllable transmission zero using only two resonant cavities. This reduces the number of reso-

nant cavities used and achieves miniaturization of the filter to some extent. The filter designed in this study has several advantages, including a simple structure, low insertion loss, wide relative bandwidth, small circuit size, and flexible and controllable transmission zeros. These features make it suitable for a variety of potential applications.

ACKNOWLEDGEMENT

This work is supported by the Chongzuo Science and Technology Program Project (No. 2023ZC1112), the School-level Research Project of Guangxi Minzu Normal University (No. 2022SP007), the Basic Research Ability Improvement Project for Young and Middle-aged Teachers in Guangxi Universities (No. 2023KY0793), and the Guangxi Natural Science Foundation (No. 2022JJB150010).

REFERENCES

[1] Bozzi, M., A. Georgiadis, and K. Wu, "Review of substrate-integrated waveguide circuits and antennas," *IET Microwaves, Antennas & Propagation*, Vol. 5, No. 8, 909–920, Jun. 2011.

[2] Chen, X.-P. and K. Wu, "Substrate integrated waveguide filter: Basic design rules and fundamental structure features," *IEEE Microwave Magazine*, Vol. 15, No. 5, 108–116, 2014.

[3] Moscato, S., C. Tomassoni, M. Bozzi, and L. Perregrini, "Quarter-mode cavity filters in substrate integrated waveguide technology," *IEEE Transactions on Microwave Theory and Techniques*, Vol. 64, No. 8, 2538–2547, Aug. 2016.

[4] Jones, T. R. and M. Daneshmand, "Miniaturized folded ridged half-mode and quarter-mode substrate integrated waveguides for filter design," *IEEE Transactions on Microwave Theory and Techniques*, Vol. 67, No. 8, 3414–3426, Aug. 2019.

[5] Qin, R., D. Zhang, Z. Ding, and M. Wang, "Duel-band filter with high out-of-band rejection using ACSRR-SIW technology," *IEICE Electronics Express*, Vol. 17, No. 12, 20190743, Jun. 2020.

[6] Shen, W., W.-Y. Yin, X.-W. Sun, and L.-S. Wu, "Substrate-integrated waveguide bandpass filters with planar resonators for system-on-package," *IEEE Transactions on Components, Packaging and Manufacturing Technology*, Vol. 3, No. 2, 253–261, Feb. 2013.

[7] Chen, X.-P. and K. Wu, "Substrate integrated waveguide cross-coupled filter with negative coupling structure," *IEEE Transactions on Microwave Theory and Techniques*, Vol. 56, No. 1, 142–149, Jan. 2008.

[8] Potelon, B., J.-F. Favennec, C. Quendo, E. Rius, C. Person, and J.-C. Bohorquez, "Design of a substrate integrated waveguide (SIW) filter using a novel topology of coupling," *IEEE Microwave and Wireless Components Letters*, Vol. 18, No. 9, 596–598, Sep. 2008.

[9] Azad, A. R., D. K. Jhariya, and A. Mohan, "Substrate-integrated waveguide cross-coupled filters with mixed electric and magnetic coupling structure," *International Journal of Microwave and Wireless Technologies*, Vol. 10, No. 8, 896–903, 2018.

[10] Shen, W., L.-S. Wu, X.-W. Sun, W.-Y. Yin, and J.-F. Mao, "Novel substrate integrated waveguide filters with mixed cross coupling (MCC)," *IEEE Microwave and Wireless Components Letters*, Vol. 19, No. 11, 701–703, Nov. 2009.

[11] You, C. J., Z. N. Chen, X. W. Zhu, and K. Gong, "Single-layered SIW post-loaded electric coupling-enhanced structure and its filter applications," *IEEE Transactions on Microwave Theory and Techniques*, Vol. 61, No. 1, 125–130, Jan. 2013.

[12] Liu, Q., D. Zhou, D. Zhang, and D. Lv, "A novel frequency-dependent coupling with flexibly controllable slope and its applications on substrate-integrated waveguide filters," *IEEE Microwave and Wireless Components Letters*, Vol. 28, No. 11, 993–995, Nov. 2018.

[13] Gong, K., W. Hong, Y. Zhang, P. Chen, and C. J. You, "Substrate integrated waveguide quasi-elliptic filters with controllable electric and magnetic mixed coupling," *IEEE Transactions on Microwave Theory and Techniques*, Vol. 60, No. 10, 3071–3078, Oct. 2012.